

REGULAR PAPER

New delay-time modulation scheme for optical pump–probe scanning tunneling microscopy (OPP–STM) with minimized light-intensity modulation

To cite this article: Osamu Takeuchi *et al* 2019 *Jpn. J. Appl. Phys.* **58** S11A12

View the [article online](#) for updates and enhancements.



New delay-time modulation scheme for optical pump–probe scanning tunneling microscopy (OPP-STM) with minimized light-intensity modulation

Osamu Takeuchi*, Hiroyuki Mogi, Zi-Han Wang, Cheul Hyun Yoon, Atsushi Taninaka, Shoji Yoshida, and Hidemi Shigekawa*

Department of Applied Physics, Faculty of Pure and Applied Sciences, University of Tsukuba, Tsukuba, Ibaraki 305-8573, Japan

*E-mail: takeuchi@bk.tsukuba.ac.jp; hidemi@ims.tsukuba.ac.jp

Received December 22, 2018; accepted February 15, 2019; published online July 8, 2019

Optical pump–probe scanning tunneling microscopy (OPP-STM) with square-wave delay-time modulation is capable of resolving nanoscale ultrafast dynamics because it does not require illumination intensity modulation that disturbs precise STM measurement. It has been overlooked, however, that when the delay time between the pump and probe pulses is modulated by periodically changing the emission timing of either the pump pulse or the probe pulse, with the other remaining the same, the illumination intensity is slightly but finitely modulated with the same periodicity as a side effect. We propose a new delay-time modulation scheme that periodically changes the emission timing of both pulses, which can greatly reduce the side effect and remove the induced fake signal in OPP-STM measurements. © 2019 The Japan Society of Applied Physics

1. Introduction

Optical pump–probe scanning tunneling microscopy (OPP-STM) with a square-wave delay-time modulation^{1–3)} is one of few successful examples^{1–10)} among a number of efforts to combine STM^{11,12)} with an optical pump–probe technique¹³⁾ for constructing a microscope that has ultimate spatial and temporal resolution at the same time. Though STM has true atomic resolution¹¹⁾ its temporal resolution is very limited. To overcome the limitation, a number of efforts have been made to improve the bandwidth of the tunnel current amplifier.^{14–16)} Today, however, commonly available tunnel current amplifiers for an ultra-high-vacuum (UHV) STM still have a temporal resolution of 1 ms to 10 μ s. Thus, even on a microsecond timescale, an OPP-STM technique is valuable while typical pump–probe measurements without a STM focus mainly on picosecond to subfemtosecond timescales.¹³⁾ Although there are a number of successful examples of time-resolved STM that do not utilize laser pulses,^{17–23)} thanks to its ultimate time resolution, OPP-STM with femtosecond laser pulses has the widest applicable range of timescales, from about 10 fs to 10 μ s.

Historically, one of the biggest problems in developing an OPP-STM has been that periodic modulation of the pump laser intensity for lock-in detection is not appropriate for OPP-STM, although it is commonly adopted in other OPP measurements without a STM. When the illumination intensity is periodically modulated, the heat arriving at the STM tip is modulated, causing thermal expansion and shrinkage of the STM tip with the same periodicity as that of the intensity modulation. Since the STM tunnel current is extremely sensitive to the tip–sample distance, the thermal expansion and shrinkage of the STM tip causes oscillation of the tunnel current at a large amplitude and hides the small time-resolved signals. Furthermore, when the thermal change in the tip length exceeds the tip–sample distance, the measurement becomes unstable due to the periodic collision of the tip and the sample.

On the other hand, lock-in detection of the STM tunnel current synchronously with square-wave delay-time modulation is effective for constructing an OPP-STM,^{1,3,14)} partly because it does not require intensity modulation. When the delay time is periodically switched between two values Δt_1

and Δt_2 and the tunnel current is lock-in detected, the in-phase lock-in output is proportional to the difference between the time-averaged tunnel currents for the two delay times, $\bar{I}_t(\Delta t_1) - \bar{I}_t(\Delta t_2)$. Here, $\bar{I}_t(\Delta t)$ represents the time-averaged tunnel current for a delay time of Δt . Thus, the delay-time dependence of the time-averaged tunnel current can be accurately obtained by sweeping Δt_1 with fixed Δt_2 .

So far, three methods are known for modulating the delay time between pump and probe pulses in OPP-STM using a square wave with a large amplitude ($\sim \mu$ s): the pulse-picker-based method,¹⁾ the pulse-generator-based method²⁾ and the triggerable pulsed-laser-based method.³⁾ In all cases, previous delay-time modulations were made by adjusting the arrival time of either the pump pulse or the probe pulse periodically, while leaving the other unchanged. Such delay-time modulation is accompanied by a slight but finite modulation of the time-averaged light intensity with the same periodicity as a side effect, especially when the delay time is modulated with a large amplitude, and this was neglected. Although a Ti:sapphire femtosecond laser can have true femtosecond time resolution, the optical setup for this costs so much that it has not been widely used. On the other hand, the recently reported pulse-generator-based method with a continuous laser and electro-optic modulator (EOM) and the triggerable-laser-based method with two externally triggerable nanosecond pulsed lasers can be built with much smaller costs (by a factor of about 100) than the pulse-picker-based method with two Ti:sapphire femtosecond lasers synchronized to each other. Because of their low cost and easier handling, the newly reported OPP-STMs are expected to be widely used by researchers in the future. Such OPP-STM measurements are negatively affected by the unwanted intensity modulation due to delay-time modulation.

In this study, we investigate in detail the intensity modulation caused by a square-wave delay-time modulation and propose a new delay-time modulation scheme that can completely suppress the out-of-phase component of the illumination intensity modulation and greatly suppress its in-phase component. The efficiency of the new scheme is confirmed by measuring the intensity itself and by applying it to measure the delay-time-dependent tunnel current from a WSe₂ sample. Though the measurement in this study was done using a triggerable-laser-based OPP-STM system, the

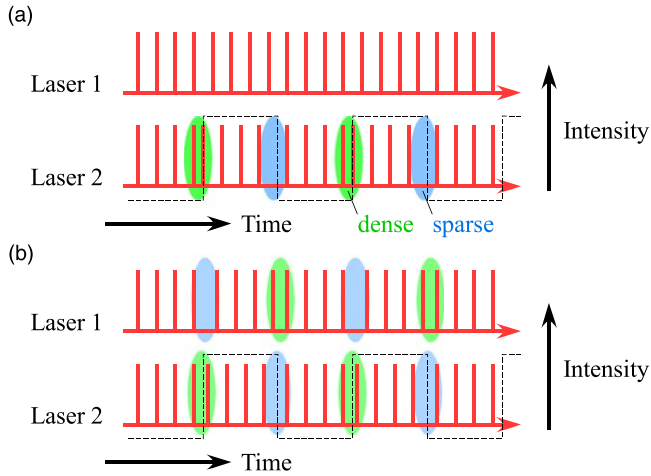


Fig. 1. (Color online) (a) Conventional square-wave delay-time modulation accompanies out-of-phase intensity modulation as a side effect. (b) In the new delay-time modulation scheme, the intensity modulations of Lasers 1 and 2 compensate each other so that the out-of-phase intensity modulation disappears.

proposed scheme is also applicable to pulse-picker-based OPP-STM and pulse-generator-based OPP-STM.

2. Intensity modulation due to delay-time modulation

First, we briefly explain how a square-wave delay-time modulation causes an intensity modulation as a side effect. In Fig. 1(a), we assume that Laser 1 emits pulses at a fixed repetition rate and the emission timing of Laser 2 is adjusted to realize the delay-time modulation. As clearly seen in the figure, the modulation of delay time causes a dense and sparse laser pulse distribution in the time domain and results in modulation of the time-averaged intensity of laser 2. Note that the intensity modulation is out of phase with the delay-time modulation by $\pi/2$. In addition, although it is difficult to see this in the figure, a small amount of in-phase intensity modulation is caused by this delay-time modulation as described in the following sections.

In an OPP-STM measurement with phase-sensitive lock-in detection, the in-phase and out-of-phase components of the tunnel current signal can be observed separately. So, even if we have a small-amplitude fake out-of-phase signal due to the unwanted intensity modulation, it does not affect the measurement of the time-resolved tunnel current signal that appears in the in-phase component. As we will see later, however, the amplitude of the out-of-phase intensity modulation can be more than 1% when large-amplitude delay-time modulation is performed. Such a large amplitude of intensity modulation may disturb the measurement, making the STM measurement unstable. Of course, OPP-STM measurement is very sensitive to in-phase intensity modulation because the fake signal induced by the modulation cannot be separated from the time-resolved tunnel current signal.

Figure 1(b) shows how the newly proposed scheme of delay-time modulation can suppress the out-of-phase intensity modulation. There, the emission timings of Lasers 1 and 2 are both shifted in opposite directions to modulate the delay time. In this case, the individual time-averaged intensities of Lasers 1 and 2 are still modulated periodically but their

polarities are opposite. Thus, the out-of-phase component of the total intensity modulation is completely nullified as long as the two lasers have the same average intensity. We will see that the small in-phase component is also reduced by half with this sequence.

To further reduce the residual in-phase component, we propose a complex delay-time modulation scheme, in which emission timings of individual pulse pairs in a period of delay-time modulation are precisely adjusted. Since complete correction requires heavy calculation to determine the amount of adjustment for each pulse pair, we also propose a simplified method for the calculation that can be done in real time with an average field-programmable gate array (FPGA) chip, which can reduce the in-phase component by a factor of about 40 compared with the conventional delay-time modulation scheme.

3. Theoretical calculation

3.1. Intensity modulation with the conventional delay-time modulation scheme

Now the above discussion is precisely studied using theoretical calculations. First, let us assume the total laser intensity can be expressed as

$$\begin{aligned}
 I(t) = & \frac{I_0}{2f_{\text{rep}}} \sum_{n=-\infty}^{\infty} \sum_{m=1}^{N_{\text{mod}}/2} \left[\delta \left(t - \Delta t_{11} - \frac{m-1/2}{f_{\text{rep}}} - \frac{n}{f_{\text{mod}}} \right) \right. \\
 & + \delta \left(t - \Delta t_{21} - \frac{m-1/2}{f_{\text{rep}}} - \frac{n}{f_{\text{mod}}} \right) \\
 & + \delta \left(t - \Delta t_{12} - \frac{m-1/2}{f_{\text{rep}}} - \frac{n+1/2}{f_{\text{mod}}} \right) \\
 & \left. + \delta \left(t - \Delta t_{22} - \frac{m-1/2}{f_{\text{rep}}} - \frac{n+1/2}{f_{\text{mod}}} \right) \right], \tag{1}
 \end{aligned}$$

where δ is the delta function, f_{rep} is the averaged laser pulse repetition rate, f_{mod} is the delay-time modulation frequency (with $N_{\text{mod}} = f_{\text{rep}}/f_{\text{mod}}$), Δt_{11} and Δt_{12} are the delay times of Lasers 1 and 2, respectively, in the first half of the modulation period, Δt_{12} and Δt_{22} are those in the second half and I_0 is the averaged total intensity. Here, it is assumed that Lasers 1 and 2 have the same intensity and that N_{mod} is an even number. The first two delta functions in Eq. (1) represent the pulses of Lasers 1 and 2 in the first half of the modulation period and the last two those in the second half. Thus, the effective delay time between Lasers 1 and 2 is $\Delta t_{21} - \Delta t_{11} = \Delta t_1$ in the first half of the modulation period and $\Delta t_{22} - \Delta t_{12} = \Delta t_2$ in the second half. Here, we assume for simplicity that the laser pulse width is short enough to be represented by the delta functions. The effect of a finite pulse width will be discussed later.

Since we are interested in the amplitude of intensity modulation due to delay-time modulation at f_{mod} , we estimate the lock-in output when the total laser intensity in Eq. (1) is lock-in detected with the reference frequency of f_{mod} . The lock-in output in the complex representation can be calculated as

$$\begin{aligned}
 I_L &= f_{\text{mod}} \int_0^{f_{\text{mod}}^{-1}} I(t) \sqrt{2} \exp(-i2\pi f_{\text{mod}} t) dt \\
 &= \frac{\sqrt{2} I_0}{2\pi} \frac{\pi/N_{\text{mod}}}{i \sin(\pi/N_{\text{mod}})} \\
 &\quad \times (e^{-i2\pi f_{\text{mod}} \Delta t_{11}} + e^{-i2\pi f_{\text{mod}} \Delta t_{21}} - e^{-i2\pi f_{\text{mod}} \Delta t_{12}} - e^{-i2\pi f_{\text{mod}} \Delta t_{22}}) \\
 &\sim \sqrt{2} I_0 f_{\text{mod}} \{ -(\Delta t_{11} + \Delta t_{21} - \Delta t_{12} - \Delta t_{22}) \\
 &\quad + i\pi f_{\text{mod}} (\Delta t_{11}^2 + \Delta t_{21}^2 - \Delta t_{12}^2 - \Delta t_{22}^2) \}.
 \end{aligned} \tag{2}$$

From this point, it is assumed for approximation that the delay times are much smaller than f_{mod}^{-1} and $1 \ll N_{\text{mod}}$. With this notation, the in-phase component with delay-time modulation corresponds to the imaginary part of I_L .

The lock-in output for the conventional scheme of the delay-time modulation between Δt_1 and Δt_2 can be calculated by substituting $\Delta t_{11} = \Delta t_{12} = 0$, $\Delta t_{21} = \Delta t_1$ and $\Delta t_{22} = \Delta t_2$ into Eq. (2) as

$$\begin{aligned}
 I_L &= \frac{\sqrt{2} I_0}{2\pi} \frac{\pi/N_{\text{mod}}}{i \sin(\pi/N_{\text{mod}})} (e^{-i2\pi f_{\text{mod}} \Delta t_1} - e^{-i2\pi f_{\text{mod}} \Delta t_2}) \\
 &\sim \sqrt{2} I_0 f_{\text{mod}} (\Delta t_2 - \Delta t_1) - i\sqrt{2} \pi I_0 f_{\text{mod}}^2 (\Delta t_2^2 - \Delta t_1^2).
 \end{aligned} \tag{3}$$

The normalized amplitude I_L/I_0 without the approximation is plotted as a function of Δt_1 in Fig. 2(a) with $\Delta t_2 = f_{\text{rep}}^{-1}/2$, $f_{\text{rep}} \sim 100$ kHz, $f_{\text{mod}} \sim 1$ kHz and $N_{\text{mod}} = 100$. The real part, i.e. the out-of-phase component (red curve), is proportional to the delay-time modulation amplitude $\Delta t_2 - \Delta t_1$ and its magnitude is about 1.4% at most. Compared with the real part, the imaginary part (blue curve) looks almost zero in the figure. As seen from the zoomed plot (light blue curve), however, it has a finite amplitude which is almost parabolic, whose vertex is at $\Delta t_1 = 0$ and whose magnitude is about 100 times smaller than that of the real part. Precisely, the imaginary part at $\Delta t_1 = 0$ is $(\pi/4)N_{\text{mod}}^{-1}$ times the real part at $\Delta t_1 = -f_{\text{rep}}^{-1}/2$.

3.2. Reduction of the out-of-phase component

The lock-in output for the new scheme that moves pump and probe pulses in the opposite direction as illustrated in Fig. 1(b) can be calculated by substituting $\Delta t_{11} = -\Delta t_1/2$, $\Delta t_{12} = -\Delta t_2/2$, $\Delta t_{21} = \Delta t_1/2$ and $\Delta t_{22} = \Delta t_2/2$ into Eq. (2):

$$\begin{aligned}
 I_L &= \frac{\sqrt{2} I_0}{\pi} \frac{\pi/N_{\text{mod}}}{i \sin(\pi/N_{\text{mod}})} \\
 &\quad \times [\cos(2\pi f_{\text{mod}} \Delta t_1/2) - \cos(2\pi f_{\text{mod}} \Delta t_2/2)] \\
 &\sim -i \frac{\sqrt{2} \pi I_0 f_{\text{mod}}^2}{2} (\Delta t_2^2 - \Delta t_1^2).
 \end{aligned} \tag{4}$$

The normalized amplitude I_L/I_0 without the approximation is plotted as a function of Δt_1 in Fig. 2(b) with the same parameters as Fig. 2(a). The result becomes a pure imaginary number, i.e. the real part is completely nullified by this scheme as shown by the red curve. On the other hand, the imaginary part is exactly the half of that of Eq. (3) as shown by the blue and light blue curves. In the above condition, the new scheme reduces the intensity modulation amplitude $|I_L|$ from $\sim 1.4\%$ to $\sim 0.55 \times 10^{-4}$, i.e. by a factor of about 200.

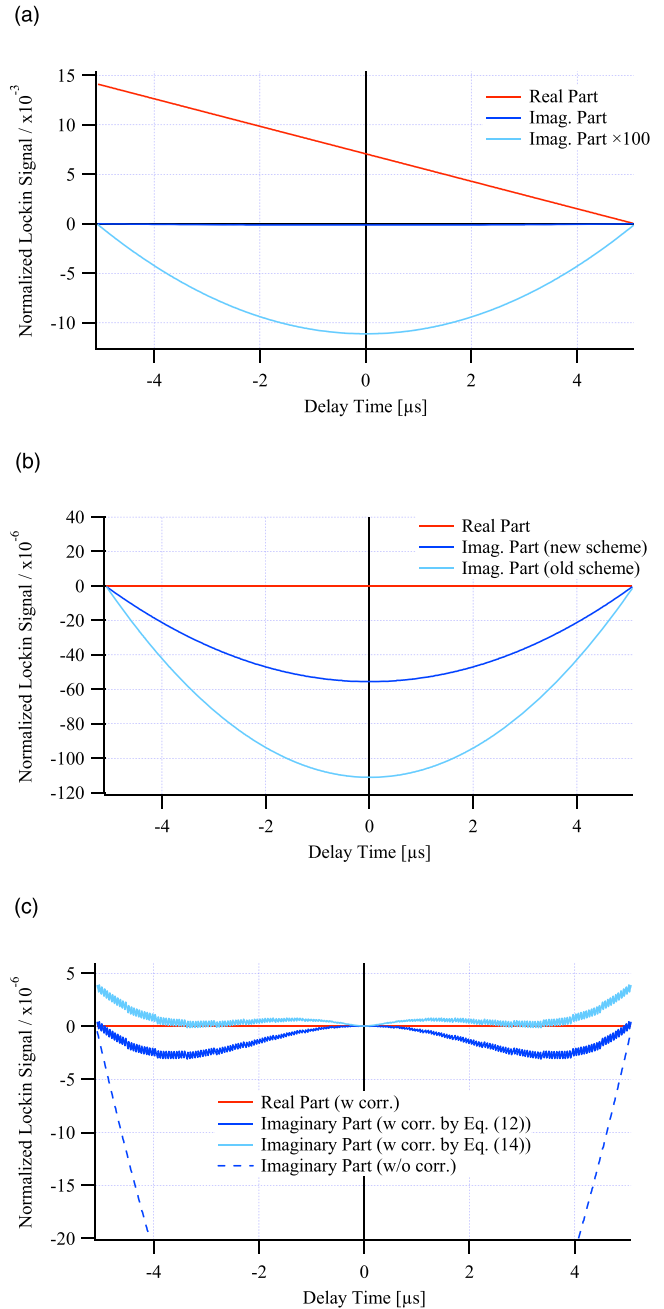


Fig. 2. (Color online) Intensity modulation amplitude due to delay-time modulation (a) for the conventional scheme and (b) for the new scheme without and (c) with correction for the residual imaginary part.

3.3. Correction for the residual in-phase component

If one wants to completely nullify both the real part and imaginary parts of I_L , Eq. (2) requires $\Delta t_{11} + \Delta t_{21} - \Delta t_{12} - \Delta t_{22} = 0$ and $\Delta t_{11}^2 + \Delta t_{21}^2 - \Delta t_{12}^2 - \Delta t_{22}^2 = 0$. This condition, however, ends up with $\Delta t_{11} - \Delta t_{12} = \Delta t_{21} - \Delta t_{22} = 0$, i.e. zero modulation amplitude. This means that we need a more complex scheme of delay-time modulation to correct for the residual in-phase component where Δt_{11} , Δt_{21} , Δt_{12} , and Δt_{22} are no longer constant in the period of delay-time modulation.

In order to correct for the component, let us assume N_{mod} is multiple of 4 and we selectively displace the emission timing of the $(N_{\text{mod}}/4 - k)$ th pulse pair by $-\Delta t$ and that of the $(N_{\text{mod}}/4 + k)$ th pulse pair by $+\Delta t$ from those in the new scheme. Then the lock-in output is altered from Eq. (4) by

$$\begin{aligned} \Delta I_L &= \frac{\sqrt{2}I_0}{iN_{\text{mod}}} \{ \cos [2\pi \{ (k - 1/2)/N_{\text{mod}} + f_{\text{mod}} \Delta t_1/2 + f_{\text{mod}} \Delta t \}] \\ &\quad - \cos [2\pi \{ (k - 1/2)/N_{\text{mod}} + f_{\text{mod}} \Delta t_1/2 \}] \\ &\quad + \cos [2\pi \{ (k - 1/2)/N_{\text{mod}} - f_{\text{mod}} \Delta t_1/2 + f_{\text{mod}} \Delta t \}] \\ &\quad - \cos [2\pi \{ (k - 1/2)/N_{\text{mod}} - f_{\text{mod}} \Delta t_1/2 \}] \} \\ &\sim \frac{i2\sqrt{2} 2\pi I_0}{N_{\text{mod}}^2} f_{\text{rep}} \Delta t \sin \frac{2\pi(k - 1/2)}{N_{\text{mod}}}. \end{aligned} \quad (5)$$

Note that such a symmetric shift of two pulse pairs makes ΔI_L a pure imaginary number. Thus, we can correct for the imaginary residue in Eq. (4) by selecting k and Δt properly.

Hereafter, we assume the delay times are controllable with $f_{\text{rep}}^{-1}/N_{\text{rep}}$ as a unit, with N_{rep} being an integer. If all pulse pairs corresponding to k are displaced by $\Delta t^{(k)} = \frac{n^{(k)}}{f_{\text{rep}} N_{\text{rep}}}$, the total difference in I_L can be written as

$$\Delta I_L \sim \frac{i2\sqrt{2} 2\pi I_0}{N_{\text{mod}}^2 N_{\text{rep}}} \sum_{k=1}^{N_{\text{mod}}/4} n^{(k)} \sin \frac{2\pi(k - 1/2)}{N_{\text{mod}}}. \quad (6)$$

Given $\Delta t_1 = \frac{n_1}{f_{\text{rep}} N_{\text{rep}}}$ and $\Delta t_2 = \frac{n_2}{f_{\text{rep}} N_{\text{rep}}}$, we obtain

$$\begin{aligned} I_L + \Delta I_L &\sim \frac{i2\sqrt{2} 2\pi I_0}{N_{\text{mod}}^2 N_{\text{rep}}} \\ &\times \left[-\frac{n_2^2 - n_1^2}{8N_{\text{rep}}} + \sum_{k=1}^{N_{\text{mod}}/4} n^{(k)} \sin \frac{2\pi(k - 1/2)}{N_{\text{mod}}} \right]. \end{aligned} \quad (7)$$

Thus, by fully optimizing all the values of $n^{(k)}$, $|I_L + \Delta I_L|$ can be reduced to be smaller than the coefficient of $n^{(1)}$,

$$\frac{2\sqrt{2} 2\pi I_0}{N_{\text{mod}}^2 N_{\text{rep}}} \sin \frac{\pi}{N_{\text{mod}}} \sim \frac{\sqrt{2} (2\pi)^2 I_0}{N_{\text{mod}}^3 N_{\text{rep}}}. \quad (8)$$

When $f_{\text{rep}} = 100$ kHz and $f_{\text{mod}} = 1$ kHz with a delay-time resolution of 5 ns, it follows that $N_{\text{rep}} = 2000$ and $N_{\text{mod}} = 100$. Thus, Eq. (8) gives $\sim 2.8 \times 10^{-8} I_0$, which can be regarded as zero in almost all applications.

In a practical experiment, however, it is often too complex, and also not required, to fully optimize the values of $n^{(k)}$. Therefore, we propose a simplified scheme to easily select values of $n^{(k)}$, which can reduce the imaginary component in Eq. (4) by a factor of about 40. First, we choose $n_2 = N_{\text{rep}}/2$. Then, the maximum of $|I_L|$ is at $n_1 = 0$. There,

$$-\frac{n_2^2 - n_1^2}{8N_{\text{rep}}} = -\frac{N_{\text{rep}}}{32}. \quad (9)$$

On the other hand, when we let $n^{(k)} = n$ for all k ,

$$\sum_{k=1}^{N_{\text{mod}}/4} n^{(k)} \sin \frac{2\pi(k - 1/2)}{N_{\text{mod}}} = \frac{n}{2 \sin \frac{\pi}{N_{\text{mod}}}}. \quad (10)$$

So, if we select n , N_{rep} , and N_{mod} to meet

$$n = \frac{N_{\text{rep}}}{16} \sin \frac{\pi}{N_{\text{mod}}}, \quad (11)$$

$I_L + \Delta I_L$ is nullified at $n_1 = 0$. For example, when $N_{\text{mod}} = 100$ and $N_{\text{rep}} = 2036$, Eq. (11) gives $n \sim 3.997$. Thus, with $n = 4$, $|I_L + \Delta I_L|$ becomes more than three orders of magnitude smaller than $|I_L|$ at $n_1 = 0$.

When $n_1 \neq 0$, $|I_L|$ increases parabolically according to Eq. (7). Taking the similarity of a parabolic function and a cosine function into account, we can correct for the parabolic

in-phase component with reasonable accuracy by setting

$$n^{(k)} = \begin{cases} 0 & k < \lfloor |n_1| N_{\text{mod}} / (2N_{\text{rep}}) \rfloor + 1 \\ n - \lfloor n \text{ frac}(|n_1| N_{\text{mod}} / (2N_{\text{rep}})) \rfloor & k = \lfloor |n_1| N_{\text{mod}} / (2N_{\text{rep}}) \rfloor + 1 \\ n & \lfloor |n_1| N_{\text{mod}} / (2N_{\text{rep}}) \rfloor + 1 < k, \end{cases} \quad (12)$$

where $\text{frac}(\cdot)$ denotes the fractional part function and $\lfloor \cdot \rfloor$ denotes the floor function. Note that, when $1 \ll N_{\text{mod}}$, the summation in Eq. (6) can be represented by a cosine function as

$$\begin{aligned} &\sum_{k=\lfloor |n_1| N_{\text{mod}} / (2N_{\text{rep}}) \rfloor}^{N_{\text{mod}}/4} n \sin \frac{2\pi(k - 1/2)}{N_{\text{mod}}} \\ &\sim n N_{\text{mod}} \int_{\lfloor |n_1| / (2N_{\text{rep}}) \rfloor}^{1/4} \sin 2\pi x dx = \frac{N_{\text{rep}}}{32} \cos(\pi n_1 / N_{\text{rep}}). \end{aligned} \quad (13)$$

For example, the normalized lock-in output $(I_L + \Delta I_L)/I_0$ without approximation is plotted as a function of Δt_1 with $n = 4$, $N_{\text{rep}} = 2036$, $N_{\text{mod}} = 100$ and a delay-time resolution of 5 ns in Fig. 2(c). The real part is unchanged from zero, as shown by the red curve. The imaginary part becomes zero at $\Delta t_1 = 0$ and $\Delta t_1 = \pm f_{\text{rep}}^{-1}/2$, as shown by the blue curve. In between, it has small negative values which approximately correspond to the difference between a parabolic function and a cosine function. As a result, with this correction, the residual imaginary part is reduced from 1.1×10^{-4} to 2.7×10^{-6} , i.e. by a factor of about 40.

With smaller N_{mod} , approximation of the summation by a cosine function that is used in Eq. (13) becomes poor. Even so, the above scheme makes $I_L + \Delta I_L$ zero at $\Delta t_1 = 0$ and $\Delta t_1 = \pm f_{\text{rep}}^{-1}/2$. In between, the residue is also reduced by a factor of about 40, although the delay-time dependence differs from that in Fig. 2(c).

Some additional optimization may be possible, depending on the conditions. When Eq. (12) is slightly modified to

$$n^{(k)} = \begin{cases} 0 & k < \lfloor |n_1| N_{\text{mod}} / (2N_{\text{rep}}) \rfloor \\ n - \lfloor n \text{ frac}(|n_1| N_{\text{mod}} / (2N_{\text{rep}})) \rfloor & k = \lfloor |n_1| N_{\text{mod}} / (2N_{\text{rep}}) \rfloor \\ n & \lfloor |n_1| N_{\text{mod}} / (2N_{\text{rep}}) \rfloor < k, \end{cases} \quad (14)$$

by omitting “+1” in the specification of the range of k , the residual in-phase component becomes much smaller in the range of delay time $|\Delta t_1| < 4 \mu\text{s}$, as shown by the light blue curve in Fig. 2(c). This “optimization,” however, only works for a finite range of N_{mod} . Note that, especially for a small N_{mod} , Eq. (14) can give a very poor result.

3.4. Different intensities for pump and probe pulses

So far we have assumed that the intensities of Lasers 1 and 2 are exactly the same. On the other hand, if they have different intensities I_1 and I_2 , the lock-in output for the conventional

scheme, Eq. (3) becomes

$$I_L = \frac{\sqrt{2} I_2}{\pi} \frac{\pi/N_{\text{mod}}}{i \sin(\pi/N_{\text{mod}})} (e^{-i2\pi f_{\text{mod}} \Delta t_1} - e^{-i2\pi f_{\text{mod}} \Delta t_2}) \sim 2\sqrt{2} I_2 f_{\text{mod}} (\Delta t_2 - \Delta t_1) - i2\sqrt{2} \pi I_2 f_{\text{mod}}^2 (\Delta t_2^2 - \Delta t_1^2). \quad (15)$$

This is same as Eq. (3) except that $I_0/2$ in Eq. (3) becomes I_2 in Eq. (15). On the other hand, the lock-in output for the new scheme without the correction, Eq. (4), becomes

$$I_L = \frac{\sqrt{2}}{\pi} \frac{\pi/N_{\text{mod}}}{\sin(\pi/N_{\text{mod}})} \{ (I_1 - I_2) [\sin(\pi f_{\text{mod}} \Delta t_1) - \sin(\pi f_{\text{mod}} \Delta t_2)] - i(I_1 + I_2) [\cos(\pi f_{\text{mod}} \Delta t_1) - \cos(\pi f_{\text{mod}} \Delta t_2)] \} \sim \sqrt{2} (I_1 - I_2) f_{\text{mod}} (\Delta t_2 - \Delta t_1) - i \frac{\sqrt{2} \pi (I_1 + I_2) f_{\text{mod}}^2}{2} (\Delta t_2^2 - \Delta t_1^2). \quad (16)$$

The imaginary part is as same as Eq. (4) taking $I_0 = I_1 + I_2$ into account. In addition to this, however, a finite real part appears, which is proportional to the intensity difference between the two lasers. Since the normalized form of the real part is $\sqrt{2} \frac{I_1 - I_2}{I_1 + I_2} f_{\text{mod}} (\Delta t_2 - \Delta t_1)$, taking the requirement $-f_{\text{rep}}^{-1} \leq \Delta t_2 - \Delta t_1 \leq f_{\text{rep}}^{-1}$ into account, $\frac{I_1 - I_2}{I_1 + I_2}$ should not exceed $N_{\text{mod}}/\sqrt{2}$ times as the required relative accuracy to suppress the magnitude of the real part below the value. For example, if a relative accuracy of 10^{-5} is required with $N_{\text{mod}} = 100$, the fluctuation amplitude at f_{mod} of $\frac{I_1 - I_2}{I_1 + I_2}$ should not exceed 0.7×10^{-3} .

When the intensities of the pump and probe pulses are intentionally chosen to have different values, one can still nullify the real part of I_L by having $\Delta t_{11}/\Delta t_{21} = \Delta t_{12}/\Delta t_{22} = -I_2/I_1$ so that the weighted-average of the emission timing of each pulse pair is not changed by the delay-time modulation. Letting $\Delta t_{11} = -\Delta t_1 I_2/(I_1 + I_2)$, $\Delta t_{21} = \Delta t_1 I_1/(I_1 + I_2)$, $\Delta t_{12} = -\Delta t_2 I_2/(I_1 + I_2)$, $\Delta t_{22} = \Delta t_2 I_1/(I_1 + I_2)$, Eq. (7) becomes

$$I_L + \Delta I_L \sim \frac{i\sqrt{2} 2\pi (I_1 + I_2)}{N_{\text{mod}}^2} \times \left[-\frac{I_1 I_2}{(I_1 + I_2)^2} f_{\text{rep}}^2 (\Delta t_2^2 - \Delta t_1^2) + \sum_{k=1}^{N_{\text{mod}}/4} 2f_{\text{rep}} \Delta t^{(k)} \sin \frac{2\pi(k-1/2)}{N_{\text{mod}}} \right]. \quad (17)$$

Thus, correction for the residual imaginary part is also possible by properly selecting the timing shift for the k th pulse pairs, $\Delta t^{(k)}$.

3.5. Finite pulse width

So far, the input of the lock-in amplifier has been regarded as a sequence of delta functions. In a real experiment, however, the pulses in the signal have a finite width because of the laser pulse shape and the impulse response of the photodetector. Such a signal can be represented by convoluting $I(t)$ in Eq. (1) with the pulse shape and the impulse response. On the other hand, as illustrated in Eq. (2), I_L is the Fourier transform of $I(t)$ at f_{mod} . It is known that the Fourier transform of a convolution integral is the product of its

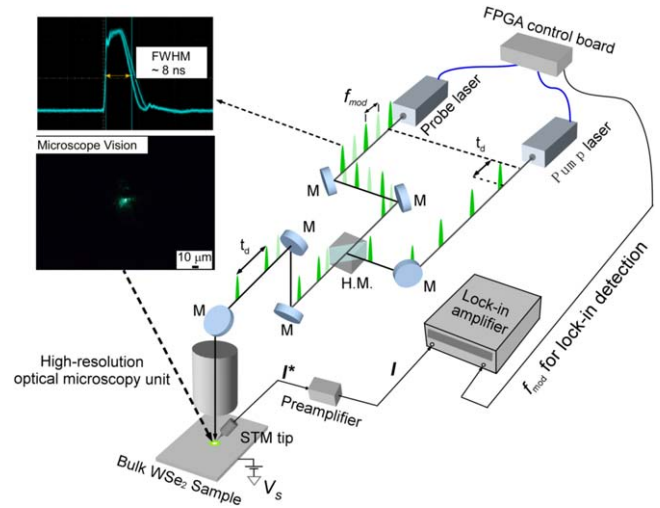


Fig. 3. (Color online) Illustration of the OPP-STM setup. Emission timings of two triggerable nanosecond pulsed lasers are controlled by a lab-built FPGA circuit to modulate the delay time between pump and probe pulses. The laser beams are coaxially aligned at a half mirror (H.M.) and illuminate the sample under STM measurement. The tunnel current signal is lock-in detected with the delay-time modulation frequency as the reference.

individual transforms. Thus, if the output of a photodetector is lock-in detected, the result will be as same as that which we obtained above except for a complex coefficient of absolute value 1 that corresponds to the product of Fourier transforms of the pulse shape and the impulse response of the photodetector, which only rotates the phase of the obtained result. Consequently, the lock-in output is independent of the pulse shape or the impulse response of the detector if the reference phase of the lock-in detection is carefully chosen to compensate for the phase rotation.

4. Experimental confirmation of the new delay-time modulation scheme

4.1. Experimental setup

Next, we confirm the efficiency of the newly proposed delay-time modulation scheme by experiments. Our OPP-STM setup is illustrated in Fig. 3. Two externally triggerable pulsed lasers, NPL52B from Thorlabs Inc., with ~ 8 ns pulse width and wavelength 520 nm are used as Lasers 1 and 2. The emission timings are controlled by a lab-built FPGA circuit implemented in a Xilinx Kintex-7 chip on the FPGA board XCM-112-160T from HuMANDATA Ltd. The internal circuit of Kintex-7 was run at a clock frequency of 200 MHz so that the emission timing could be adjusted with a resolution of 5 ns. For an OPP-STM measurement, two laser beams are coaxially aligned at a half mirror (H.M. in the figure) and focused onto the sample surface from a normal incident angle. The measurement setup was equipped with an ultra-high-vacuum multi-probe STM system from UNISOKU Co., Ltd. with lab-built electronics and software. In this system, the STM tip is tilted from the sample surface normal. Thus, the tip does not block the normal-incidence laser illumination. The tunnel current is lock-in detected with the delay-time modulation frequency as the reference.

4.2. Measurement of laser intensity

First, the total laser intensity measured by a photodiode (not shown in Fig. 3) was lock-in detected with the delay-time modulation frequency as the reference. The lock-in output is

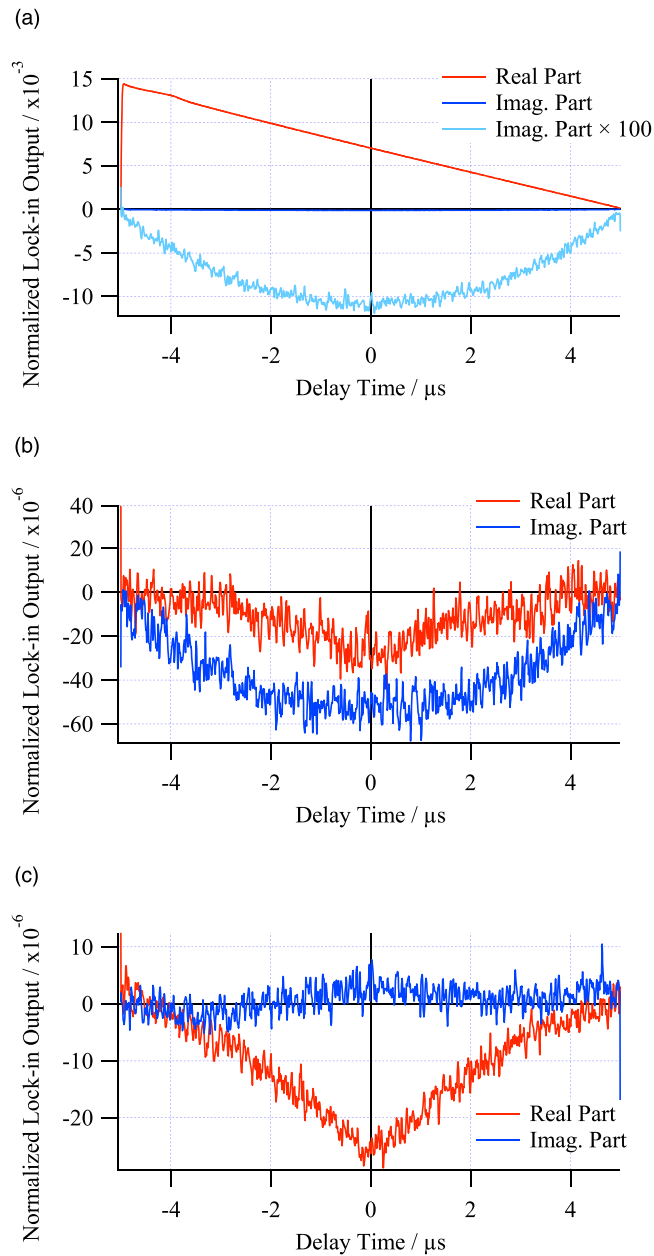


Fig. 4. (Color online) Normalized lock-in output for laser intensity measurements (a) with the old scheme, (b) with the new scheme without correction for an imaginary residue and (c) with the new scheme with correction.

averaged for multiple sweeps of the delay time and plotted as a function of Δt_1 with $N_{\text{rep}} = 2036$ and $N_{\text{mod}} = 100$, i.e. $f_{\text{rep}} \sim 100$ kHz and $f_{\text{mod}} \sim 1$ kHz with fixed $\Delta t_2 = f_{\text{rep}}^{-1}/2 = 5 \mu\text{s}$, the same as those in Fig. 2. As expected in Fig. 2(a), the conventional delay-time modulation scheme causes a large-amplitude out-of-phase component that is proportional to $\Delta t_2 - \Delta t_1$ (red curve) and the parabolic in-phase component (light blue curve) as shown in Fig. 4(a). The magnitude of these components also agrees with expectations.

With the new scheme without the precise correction, the out-of-phase component was greatly reduced as expected, as shown by the red curve in Fig. 4(b). However, some small unexpected out-of-phase component remained (red curve) while the in-phase component agrees with the expectation (blue curve). Figure 4(c) shows the result for the new scheme with correction by Eq. (12) with $n = 4$. Since we spent more

time acquiring this result the noise level is greatly reduced. As a result, the detailed shape of the unexpected component can be seen (red curve). The unexpected out-of-phase component resembles two exponential decays from $\Delta t_1 = 0$ symmetrically towards the positive and negative directions with a very long decay time ($>3 \mu\text{s}$). Since the amplitude and decay time of this component change when we replace the photodetector with another whose characteristics are different from the original one, we interpret this unexpected component as originating from the nonlinear response of the photodetector. The in-phase component (blue curve) was greatly reduced from Fig. 4(b). Consequently, it was confirmed that the newly proposed delay-time modulation scheme efficiently reduces both the in-phase and out-of-phase components of the illumination intensity modulation.

4.3. OPP-STM measurement with the new delay-time modulation scheme

Finally, OPP-STM measurement was performed with the new delay-time modulation scheme. We chose WSe_2 as the sample, which is a layered indirect-bandgap semiconductor with a relatively long carrier recombination lifetime.^{24,25} As previously reported,³ this system exhibits two exponential decay components in OPP-STM which have decay constants of $\sim 0.15 \mu\text{s}$ and $\sim 1.5 \mu\text{s}$, respectively. It was insisted that they correspond to the lifetimes of photocarriers in and out of the tip-induced depletion region.^{26,27}

The OPP-STM result with the conventional delay-time modulation scheme is shown in Fig. 5(a) with $N_{\text{rep}} = 2036$, $N_{\text{mod}} = 100$ and a delay-time resolution of 5 ns, i.e. $f_{\text{rep}} \sim 100$ kHz and $f_{\text{mod}} \sim 1$ kHz with fixed $\Delta t_2 = f_{\text{rep}}^{-1}/2 = 5 \mu\text{s}$, as in Figs. 2 and 4. The sample bias voltage V_S is -1.2 V and the reference tunnel current I_{ref} is -100 pA. In addition to the time-resolved tunnel current signal that appears in the in-phase component (blue curve), a small but distinguishable fake signal appears in the out-of-phase component (red and purple curves), which is proportional to the delay-time modulation amplitude $\Delta t_2 - \Delta t_1$. As discussed above, this fake signal is caused by unwanted intensity modulation as a side effect of the delay-time modulation. With the new modulation scheme with the precise correction by Eq. (12) with $n = 4$, this fake signal was completely removed (red and purple curves) while the time-resolved tunnel current signal was unchanged (blue curve), as shown in Fig. 5(b). In this experiment, the time-resolved tunnel current signal is so large that the effect of the in-phase intensity modulation was not observable. Note that the expected magnitude for the in-phase intensity modulation is smaller than that for the out-of-phase intensity modulation by a factor of $(4/\pi)N_{\text{mod}} \sim 127$. Thus, the in-phase fake signal in Fig. 5(a) is expected to be ~ 3 fA in this experiment.

Since the in-phase signal is proportional to N_{mod}^{-2} , when N_{mod} is smaller the fake signal indeed affects the experiment. An OPP-STM result with $N_{\text{mod}} = 8$ is shown in Fig. 5(c). Other parameters are $V_S = -1.2$ V, $I_{\text{ref}} = -200$ pA and $N_{\text{rep}} = 8332$, i.e. $f_{\text{rep}} \sim 24$ kHz and $f_{\text{mod}} \sim 3$ kHz with $\Delta t_2 = f_{\text{rep}}^{-1}/2 = 20 \mu\text{s}$. With the conventional scheme, a large fake signal appears in the real part that is proportional to the delay-time modulation amplitude (red curve). In Fig. 5(c), the delay-time-dependent tunnel current is distinguishable in the imaginary part. This is as same as in Fig. 5(b). But how it looks in Fig. 5(c) is different from

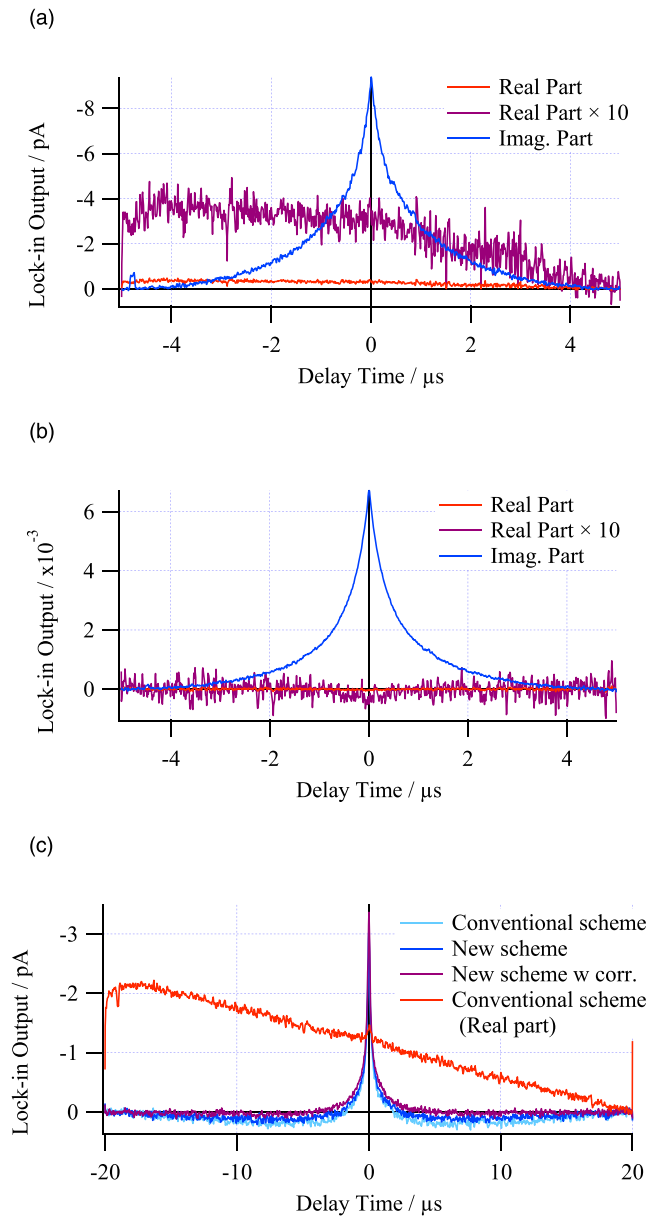


Fig. 5. (Color online) Lock-in output for OPP-STM measurements on WSe_2 (a) with the conventional scheme, (b) with the new scheme without correction by Eq. (12) and (c) with a smaller N_{mod} .

Fig. 5(b). In addition, however, the imaginary part with the conventional scheme shows a small downward bend around the delay-time origin (light blue curve). The amount of downward bending is reduced by half with the new scheme without the correction (blue curve) and becomes almost zero with the new scheme with the correction by Eq. (12) (purple curve). This downward bending is due to in-phase intensity modulation. Indeed, the relative magnitude of the fake signals in the out-of-phase and in-phase components was as expected, $(4/\pi)N_{mod} \sim 10$. Consequently, for OPP-STM measurements, the proposed delay-time modulation scheme is efficient at removing the fake signals due to unwanted intensity modulation caused as a side effect of square-wave delay-time modulation.

5. Conclusions

The unwanted intensity modulation caused as a side effect of square-wave delay-time modulation in an OPP-STM

measurement was investigated in detail. When delay-time modulation is done by shifting the emission timing of either the pump or the probe pulse while that of the other is unchanged, intensity modulation that is out-of-phase with the delay-time modulation is induced, the amplitude of which is proportional to the delay-time modulation amplitude. In addition to this, intensity modulation that is in phase with the delay-time modulation is also induced, the amplitude of which is a parabolic function of the delay time. A new delay-time modulation scheme was proposed, in which the emission timing of the pump and probe pulses are both shifted in the opposite direction to realize delay-time modulation. With this new scheme, the out-of-phase intensity modulation is completely nullified, while the in-phase intensity modulation is reduced by half. To reduce the residual in-phase intensity modulation, a correction method for the new scheme is also proposed, in which the emission timings of individual pulse pairs in a half period of the delay-time modulation are adjusted. The correction reduces the in-phase intensity modulation in the conventional scheme by a factor of about 40. It was confirmed that the corrected new scheme indeed nullifies the fake signals due to the unwanted intensity modulation in OPP-STM measurement on WSe_2 . In this study, the experiment was done with triggerable-laser-based OPP-STM. However, the proposed scheme is also applicable to pulse-picker-based OPP-STM or pulse-generator-based OPP-STM.

Acknowledgments

Support from Japan Society for the Promotion of Science (Grants-in-Aid for Scientific Research: 15H02023 and 17H06088) is acknowledged.

- 1) Y. Terada, M. Aoyama, H. Kondo, A. Taninaka, O. Takeuchi, and H. Shigekawa, *Nanotechnology* **18**, 044028 (2007).
- 2) P. Kloth and M. Wenderoth, *Sci. Adv.* **3**, e1601552 (2017).
- 3) H. Mogi, Z.-H. Wang, R. Kikuchi, C. H. Yoon, S. Yoshida, O. Takeuchi, and H. Shigekawa, *Appl. Phys. Express* **12**, 025005 (2019).
- 4) M. R. Freeman, A. Y. Elezabi, G. M. Steeves, and G. Nunes Jr., *Surf. Sci.* **386**, 290 (1997).
- 5) O. Takeuchi, M. Aoyama, R. Oshima, Y. Okada, H. Oigawa, N. Sano, H. Shigekawa, R. Morita, and M. Yamashita, *Appl. Phys. Lett.* **85**, 3268 (2004).
- 6) A. Dolocan, D. P. Acharya, P. Zahl, P. Sutter, and N. Camillone III, *J. Phys. Chem. C* **115**, 10033 (2011).
- 7) S. Dey, D. Mirell, A. R. Perez, J. Lee, and V. A. Apkarian, *J. Chem. Phys.* **138**, 154202 (2013).
- 8) T. L. Cocker, V. Jelic, M. Gupta, S. J. Molesky, J. A. J. Burgess, G. De Los Reyes, L. V. Titova, Y. Y. Tsui, M. R. Freeman, and F. A. Hegmann, *Nat. Photon.* **7**, 620 (2014).
- 9) S. Yoshida, Y. Aizawa, Z.-H. Wang, R. Oshima, Y. Mera, E. Matsuyama, H. Oigawa, O. Takeuchi, and H. Shigekawa, *Nat. Nanotechnol.* **9**, 588 (2014).
- 10) J. Sakai, S. Katano, M. Kuwahara, and Y. Uehara, *J. Phys.: Condens. Matter* **29**, 405001 (2017).
- 11) G. Binnig, H. Rohrer, C. Gerber, and E. Weibe, *Phys. Rev. Lett.* **49**, 57 (1982).
- 12) C. J. Chen, *Introduction to Scanning Tunneling Microscopy* (Oxford University Press, Oxford, 2007).
- 13) J. Shah, *Ultrafast Spectroscopy of Semiconductors and Semiconductor Nanostructures* (Springer, Berlin, 1999).
- 14) H. J. Mamin, H. Birk, P. Wimmer, and D. Rugar, *J. Appl. Phys.* **75**, 161 (1994).
- 15) J. Wintterlin, J. Trost, S. Renisch, R. Schuster, T. Zambelli, and G. Ertl, *Surf. Sci.* **394**, 159 (1997).
- 16) U. Kemiktarak, T. Ndukum, K. C. Schwab, and K. L. Ekinci, *Nature* **450**, 85 (2007).

- 17) S. Grafström, *Appl. Phys. Rev.* **9**(1), 1717 (2002).
- 18) S. Loth, M. Etzkorn, C. P. Lutz, D. M. Eigler, and A. J. Heinrich, *Science* **329**, 1628 (2010).
- 19) I. Moul, M. Herve, and Y. Pennec, *Appl. Phys. Lett.* **98**, 233103 (2011).
- 20) C. Saunusa, J. R. Bindel, M. Pratzner, and M. Morgenstern, *Appl. Phys. Lett.* **102**, 051601 (2013).
- 21) T. L. Cocker, D. Peller, P. Yu, J. Repp, and R. Huber, *Nature* **539**, 263 (2016).
- 22) K. Yoshioka, I. Katayama, Y. Minami, M. Kitajima, S. Yoshida, H. Shigekawa, and J. Takeda, *Nat. Photon.* **10**, 762 (2016).
- 23) V. Jelic, K. Iwaszczuk, P. H. Nguyen, C. Rathje, G. J. Hornig, H. M. Sharum, J. R. Hoffman, M. R. Freeman, and F. A. Hegmann, *Nat. Phys.* **13**, 591 (2017).
- 24) L. C. Upadhyayula, J. J. Loferski, A. Wold, W. Giriat, and R. Kershaw, *J. Appl. Phys.* **39**, 4736 (1968).
- 25) M. K. Agarwal and P. A. Wani, *Mater. Res. Bull.* **14**, 825 (1979).
- 26) M. Feenstra, Y. Dong, M. P. Semtsiv, and W. T. Masselink, *Nanotechnology* **18**, 044015 (2007).
- 27) S. Yoshida, J. Kikuchi, Y. Kanitani, O. Takeuchi, H. Oigawa, and H. Shigekawa, *e-J. Surf. Sci. Nanotechol.* **4**, 192 (2006).